Appl. Phys. A 80, 753–758 (2005)
DOI: 10.1007/s00339-004-3081-4

Applied Physics A
Materials Science & Processing

J.-P. SYLVESTRE
A.V. KABASHIN
E. SACHER
M. MEUNIER✉

Femtosecond laser ablation of gold in water: influence of the laser-produced plasma on the nanoparticle size distribution

Laser Processing Laboratory, Department of Engineering Physics, Ecole Polytechnique de Montréal, Case Postale 6079, succ. Centre-ville, Montréal, Québec, Canada, H3C 3A7

Received: 15 July 2004/Accepted: 29 September 2004
Published online: 15 December 2004 • **© Springer-Verlag 2004**

ABSTRACT Femtosecond laser radiation has been used to ablate a gold target in pure deionized water to produce gold colloids. The dimensional distribution of nanoparticles is characterized by the simultaneous presence of two distinct particle populations: one with low dispersion, having a mean particle size of 5–20 nm, and one with high dispersion, having a much larger particle size. By changing the target position with respect to the radiation focus, we study the influence of the plasma formed after the laser pulse in front of the target, during nanofabrication process. We show that the most intense plasma is produced by positioning the target slightly before the geometric focal point. Here, the plasma intensity was found to correlate with the amount of ablated material as well as with the mean size of nanoparticles associated with the second, highly dispersed, distribution of nanoparticles; this suggests the involvement of plasma-related processes in the ablation of material, and the formation of relatively large particles. The thermal heating of the target by the plasma, and its mechanical erosion by the collapse of a plasma-induced cavitation bubble are discussed as possible ablation mechanisms. The gold nanoparticles produced in ultrapure water are of importance for biosensing applications.

PACS 81.07.-b; 81.16.-c

1 Introduction

Nanoparticles of noble metals are predicted to be, or are already, successfully employed in a wide range of applications, including catalysis, nanoelectronics and, particularly, biosensing. Gold nanoparticles (< 30 nm) are particularly interesting for these tasks since they are chemically stable and strongly absorb light around 520 nm, due to the presence of a resonant surface plasmon excitation [1]. Over the last decade, the major effort has been on the production of stable solutions of small nanoparticles with narrow size distributions and controlled surface chemistry. Although 5–100 nm nanoparticles can be produced by a relatively simple chemical reduction method [2], the surface of these nanoparticles is likely to be contaminated with reaction by-products such as anions and reducing agents, which can interfere with subsequent stabilization and functionalization steps.

✉ Fax: +1-514-340-3218, E-mail: michel.meunier@polymtl.ca

The laser ablation of a noble metal target immersed in a liquid was introduced as an alternative physical method for colloidal nanoparticle fabrication [3–19]. In contrast to the chemical reduction method, laser ablation offers the possibility of nanoparticle growth in a controllable, contamination-free environment, a key requirement for the subsequent successful functionalization of the nanoparticle surface. To reduce the size and size dispersion of nanoparticles produced by laser ablation, their growth has been controlled by both chemical and physical methods. The chemical approach consists of the addition of specific molecules, capable of interacting physically or chemically with the surface of the forming particles, to the liquid fabrication environment to limit their subsequent coalescence. In particular, an efficient size reduction was observed by the use of ionic surfactants [6–10], although they are not always suited for biosensing applications because of biocompatibility problems. Much more biocompatible cyclodextrins (torus-like macrocycles built up of glucose pyranose units [20]) appear more promising for the size reduction tasks providing nanoparticles with a mean size of 2–2.5 nm and a size dispersion of 1–1.5 nm [11, 12]. In contrast, the physical size control approach employs variations of physical parameters to control the nanoparticle growth. Although limited size reductions can be achieved with nanosecond laser pulses [8, 16], femtosecond radiation gave much more efficient size control, permitting mean size particle variations between 4 to 150 nm [18]. Basically, nanofabrication with femtosecond radiation was characterized by the presence of two populations of nanoparticles. The first contained particles with a relatively small mean size (4–15 nm) and a narrow dispersion (8–10 nm FWHM), whereas the second had particles with a much larger mean size (15–130 nm) and a broader size dispersion (20–90 nm FWHM) [18]. Although the data indicate the involvement of radiation- and plasma-related mechanisms of material ablation, many aspects of the phenomenon remain unclear.

This paper also focuses on the femtosecond laser ablation of gold in water. We vary the position of the target with respect to the focal plane of a focusing objective, permitting not only the variation of the radiation fluence, but also the control of the position of the laser-produced plasma with respect to the target. In order to clarify the role of the plasma in the nanofabrication process, we examine the target mass loss, the sound and visible emission from the plasma, and the concen-

tration of nanoparticles, in addition to the size distribution of the nanoparticles.

2 Experimental section

2.1 *Femtosecond laser ablation*

Laser ablation was carried out with a Ti/sapphire laser (Hurricane, Spectra Physics Lasers), which provides 120 fs FWHM pulses (wavelength 800 nm, maximum energy 1 mJ/pulse, repetition rate 1 kHz, beam diameter 7 mm). The radiation was focused by an objective with a focal length of 7.5 cm onto a gold target, forming a focal spot of about 6 μm. The target was placed on the bottom of a 3-mL glass vessel filled with high-purity deionized water (18 MΩ cm), as shown in Fig. 1. The height of the water layer above the gold was 12 mm. The vessel was placed on a horizontal platform, which revolved at a constant speed of 0.5 mm/s to form circle-like ablated regions on the target surface. A gold rod (99.99%, Alfa Aesar), with a diameter of 6 mm, was used as the target. The upper surface of the rod was polished prior to each experiment, to provide identical ablation conditions in different experiments. The height of the water layer above the gold was 12 mm.

The position of the target surface with respect to the focal plane of the objective was the main variable parameter in our experiments. The zero point ($Z = 0$) corresponded to the focal plane at the target surface. This point was determined from a scanning electron microscopic (SEM, model Phillips XL20) analysis of craters on the gold, using a relatively low laser pulse energy (0.25 μJ) to avoid plasma heating and self-focusing or filamentation effects [21]. In the experiments, the position of the focusing objective was shifted over the Z-axis, and the laser energy was kept constant at 0.25 mJ/pulse, resulting in a laser fluence at the focal point of about 880 J/cm^2. To simplify the interpretation of the results, we will consider all manipulations relative to the system of coordinates connected to the objective focal plane. Consequently, target positions before and beyond the objective focus will correspond to positive and negative values of Z, respectively, as shown in Fig. 1.

2.2 *Measurements*

Measurement parameters were tightly controlled during and after the ablation process. The sound generated was recorded using a microphone connected to a computer. The gold target mass loss was calculated by measuring the mass of the target before and after 20 minutes of ablation, using a microbalance. The craters formed on the target surface were examined by SEM. Absorption spectra of the colloidal solutions were measured just after their production, in the spectral region 350–800 nm, using a Lambda 19 UV-VIS spectrometer (Perkin Elmer). A transmission electron microscope (Philips CM30), with 0.23 nm point-to-point resolution, was used to obtain micrographs of the gold nanoparticles. A drop of sample solution was placed on a carbon-coated, Formvar-covered copper grid, and dried at room temperature. Typically, the diameters of 500–1000 particles observed on a given micrograph were measured and the particle size (diameter) distribution was calculated.

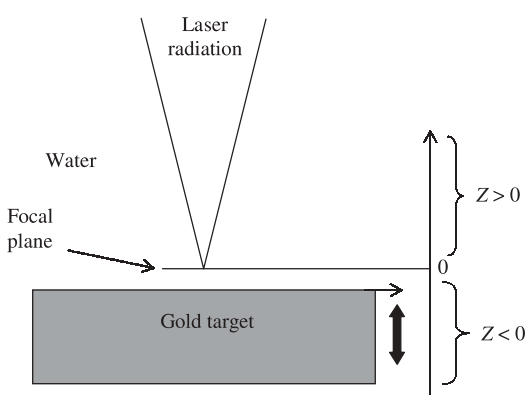

FIGURE 1 Schematic of the experimental setup

3 Results

In our experiments, laser ablation of the gold target in water was accompanied by the production of a plasma plume, visible to the eye, near the target surface; in addition, a sharp sound was heard, which is usually attributed to the collapse of the cavitation bubble in the liquid, formed as a result of the vaporization of a water layer in contact with the plasma [22, 23]. Under fixed laser energy, the intensities of both the plasma emission and the sound increased as the target approached the focal plane ($Z = 0$), as shown in Fig. 2a. However, the most intense sound and plasma emission were recorded when the target surface was slightly in front of the focal plane, at $Z_{max} = +400$–500 μm (Fig. 2a). As we found from target mass measurements, in which target mass characteristics were measured after 20 minutes of laser ablation, maximal mass loss took place during the most intense plasma emission and sound, strongly suggesting that the ablation of material relates to the plasma intensity (Fig. 2b).

The color of the colloidal solutions also depended on the intensities of plasma emission and sound. The sols appeared dark red, with some yellow metallic tint, when the target was near $Z = Z_{max}$. Such sols strongly scattered incident light, while some nanoparticles from the solution tended to precipitate to form a gold-colored layer at the bottom of the glass vial several hours after fabrication, suggesting the presence of large nanoparticles in the sol. In contrast, far from this point of Z_{max}($Z > 1500$ μm, $Z < -500$ μm) the sols had a clear red or pink color and were stable for several weeks, suggesting the formation of smaller particles. Absorption spectra of the solutions were characterized by the presence of a peak around 520–530 nm (Fig. 3), attributed to the resonant excitation of surface plasmons in individual gold nanoparticles with sizes from 3 to 60 nm; the intensity of this peak is known to be proportional to the concentration of nanoparticles in this range [7–9]. Therefore, using the data on radiation absorption, we can estimate the concentration of relatively small nanoparticles in sols prepared at various target positions. As shown in Fig. 2c, the maximal concentration of small nanoparticles was obtained at $Z_{conc.\ max} = +700$ μm, which is close to Z_{max}. The slight difference between $Z_{conc.\ max}$ and Z_{max} is probably explained by the fact that laser ablation at Z_{max} provides much larger nanoparticles, which do not absorb in the wavelength range of 520–530 nm.

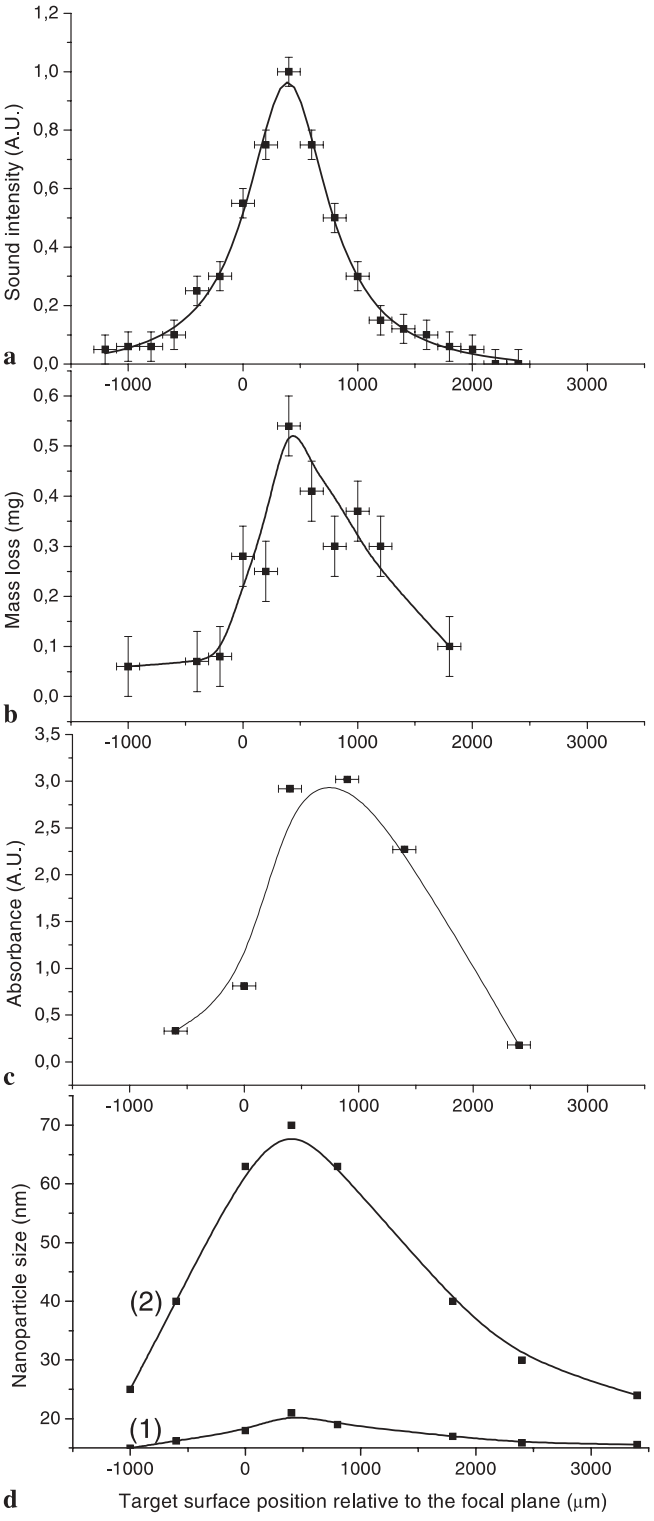

FIGURE 2 (**a**) Sound intensity, (**b**) mass loss of the gold target (**c**) concentration of the gold colloids estimated from absorption spectra and (**d**) size distribution maxima for low (1) and highly (2) dispersed populations of colloids, as a function of the target position with respect to the lens focal plane ($Z = 0$)

As in our previous work [18], TEM studies of nanoparticle production confirmed the presence of two populations. Figure 4 presents a typical TEM micrograph and the corresponding size statistics for a sample fabricated near $Z = 0$.

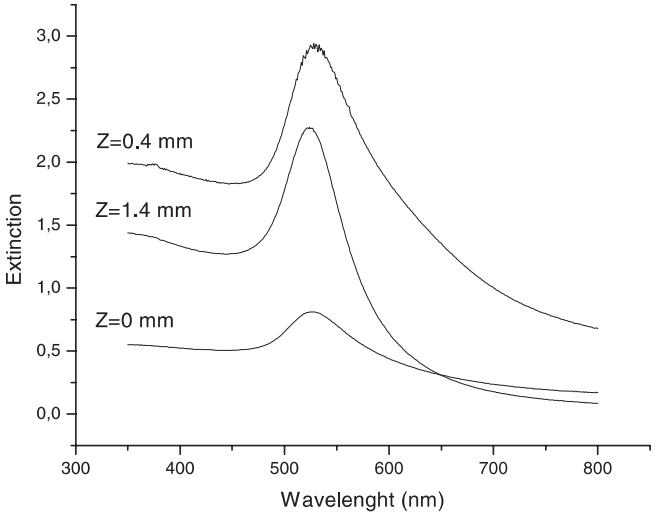

FIGURE 3 Extinction spectra of gold sols prepared by femtosecond laser ablation in water at various target positions

As shown in the figure, a sharp peak around 10–20 nm and a broad, slowly decreasing tail characterized the size distribution. Such a distribution requires a superposition of two Gaussian functions, as shown in Fig. 4. Here, the net distribution appears to be a combination of a less dispersed population of particles with a mean particle size value close to the net distribution maximum, and a relatively broad, highly dispersed one with much larger mean particle size. Figure 2d presents the mean size, corresponding to maxima of the (1) low- and (2) highly dispersed distributions, as a function of the target surface position along the Z-axis. As shown in the figure, the mean nanoparticle size increases as the target approaches the point of the most intense plasma intensity, at $Z = 400\,\mu\text{m}$. However, the size dependence appears to be much more prominent for the highly dispersed particle population compared to the less dispersed one. Indeed, the change of the target position from 3000 μm to 400 μm led to a sig-

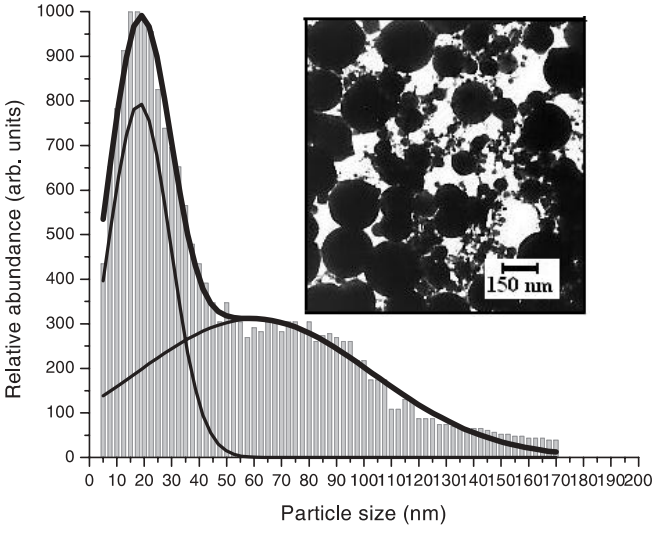

FIGURE 4 TEM micrograph image and corresponding size distribution of gold nanoparticles prepared by the femtosecond laser ablation, when the target surface was at the geometric focus of the objective ($Z = 0$)

nificant shift of the distribution maximum from 23 to 70 nm for the highly dispersed population, while the relevant shift for the less dispersed one was much weaker, from 15 to 19 nm. We also noticed that the relative intensity of the peak, associated with the highly dispersed distribution, decreased as the target moved away from Z_{max}. In fact, such a moving away from the focal plane corresponded to a decrease of laser fluence on the target surface. Note that a similar decrease of intensity of the highly dispersed distribution or even its complete disappearance was observed in our experiments on decreasing the laser energy under fixed target positioning [18].

Typical craters on the gold target, as seen by SEM after 1000 laser pulses, are found in Fig. 5. As shown in the figure, craters are not found when the target surface is far from the focal plane. In this case, ablation leads to the simple removal of the upper surface layer without any indication of melting effects (Fig. 5a). In contrast, positioning the target near the plasma intensity maximum leads to clearly visible craters, whose walls contain traces of molten material (Fig. 5b). Note that crater profiles can broaden somewhat, due to the change of the spot position on the target surface, as a result of a perturbation of the water layer, leading to a change of its refraction conditions.

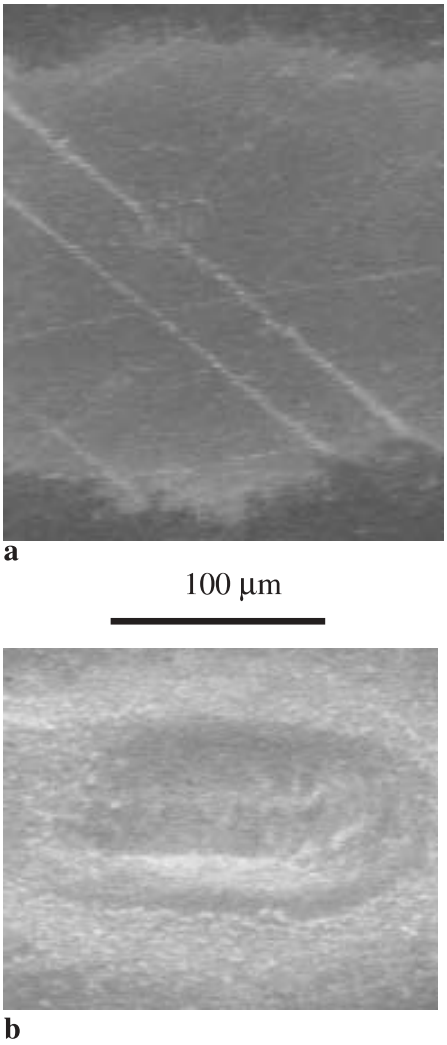

FIGURE 5 SEM images of craters obtained after 1000 laser pulses for the target position at (**a**) $Z = +2500$ μm and (**b**) $Z = +400$ μm, corresponding to the plasma intensity maximum. The scratches are due to post-ablation target manipulation

4 Discussion

When the femtosecond radiation acts on a solid target, the radiation energy is known to be absorbed by the target itself. Then, several picoseconds after the laser pulse [24] the radiation-related ablation of material takes place, yielding to the ejection of atoms and small clusters [25, 26]. The nanoclusters tend to coalesce during their subsequent cooling in the ambient medium, forming particles in the nanometer range. However, when the radiation fluence is high enough, additional factors related to the presence of the plasma must be taken into account. Basically, the plasma can be formed as the result of the ablation of material from the target or through the optical breakdown of water induced by the femtosecond radiation. In the latter case, the radiation is readily absorbed in water due to non-linear phenomena and a plasma is formed in front of the target surface. Absorbing up to 70% of the laser power [22], the optical breakdown phenomenon decreases the efficiency of pure radiation-related ablation. In our view, the plasma can become intense enough to produce the additional ablation of material, independent of the method of plasma production (direct material ablation or water breakdown production). This may be due to thermal melting of the target surface on contacting the hot plasma [18]. In addition, the laser-provoked initiation of plasma in liquid is accompanied by the production of bubbles, formed as a result of the water vaporization on contacting the hot plasma [22, 23]. The bubbles quickly merge to form a single larger bubble, known as the cavitation bubble. The collapse of the cavitation bubble, taking place 50–150 μs after the plasma initiation, is accompanied by a significant release of energy [22]. We reason that this energy is large enough to cause a secondary ablation of material.

In our experiments, we changed the target position with respect to the objective focal plane. In fact, the shift of the target (along the Z-axis) from the focal plane, corresponds to an enlargement of the irradiation spot on the surface, which, in turn, decreases the laser fluence. In addition, the defocusing changes the position of the laser-produced plasma with respect to the target. Indeed, when the target is before the focal plane, the plasma can be formed uniquely by ablated material from the target, or by the ablated material in combination with the breakdown-induced plasma in water, leading to different distances between the center of the plasma initiation and the target surface. Furthermore, when the target is beyond the focal plane, two centers of plasma production take place: the first one, localized near the focal point, is much stronger and is related to the breakdown of water, while the second one, associated with the ablated material, is near the target surface. In this case, the two plasmas can be completely separated under the positioning of the target at some point relatively far the focal plane. Note that the plasma intensity, recorded by sound and optical emission from the plasma, is greatest when the target is slightly in front of the focal plane. This is probably explained by the phenomenon of self-focusing, which can play an important role at relatively high laser intensities.

Self-focusing tends to narrow the beam diameter as the laser pulse moves through the aqueous medium, giving rise to the focusing of the beam before the geometric focal plane of the objective [27]. The point of greatest plasma intensity probably corresponds to conditions of radiation focusing on the target surface.

As in [18], our experiments revealed the presence of two populations of nanoparticles produced by ablation. The first, less dispersed, population was characterized by a relatively small mean nanoparticle size, which decreased only slightly when the target moved away from the point of maximal plasma intensity $Z = Z_{max}$. Furthermore, this population could be efficiently produced even in a region far from the point of Z_{max} (before or beyond the focal plane). Since the ablation in this region is characterized by the absence of target melting effects, as shown in Fig. 5a, it can be attributed to the pure radiation-based ablation of nanoclusters and their subsequent coalescence in the water environment. Indeed, the absence of melting effects is consistent with a significant reduction, or the complete removal, of the heat-affected zone; this is the essential feature of the femtosecond laser ablation due to the shortness of the laser pulse compared to the heat diffusion time [24]. In contrast, the fabrication of the second, highly dispersed, population of nanoparticles was efficient only under the production of a strong plasma, when the target was near Z_{max}. Furthermore, the ablation of material was accompanied by the formation of craters with traces of molten material, as shown in Fig. 5b. Taking into account the absence of melting effects under the femtosecond laser ablation, these craters can only be explained by the involvement of plasma-related processes. As we have already discussed, target heating by the plasma or its erosion through the collapse of the cavitation bubble could be possible mechanisms of the plasma-related ablation of material. The plasma-related origin of the highly-dispersed population is confirmed by the fact that the increase of the plasma intensity leads to the simultaneous increase of the target mass loss and the mean size of nanoparticles of the highly dispersed population, as shown in Fig. 2. Indeed, the increase of the plasma intensity enhanced the efficiency of plasma-related mechanisms of material ablation, which, in turn, led to higher concentration of ablated particles, increasing the efficiency of the process of their coagulation. Another evidence for the plasma-related origin of this population follows from the geometry of the experiment. One may see from Fig. 2a that the decrease of plasma sound signal was almost the same when the target moved away from Z_{max} in either direction. A similar effect was observed for the plasma emission intensity, suggesting that it is approximately the same when the target is placed at symmetrical distances from Z_{max}. However, as shown in Fig. 2b,d, the decrease of the mass loss and the mean size of nanoparticles are much more rapid when the target moves beyond the focal plane. Taking into account that the water breakdown-related loss of the radiation energy is almost the same under the target positions at symmetrical distances from Z_{max}, the rapid decrease can be explained by the detachment of the breakdown-related plasma from the target, which leads to the decrease of the efficiency of the plasma-related ablation.

As a final comment, in order to produce fine nanoparticles by laser ablation in pure water, our results suggest that one should avoid plasma-related ablation and favour pure laser ablation. With a femtosecond laser, this can readily be achieved, for example, by using low laser energy and/or out-of-focus conditions, as shown in our previous studies [18] and in this paper. In contrast, the fabrication of fine (< 10 nm) Au particles by the nanosecond laser ablation of a bulk target in pure water still needs to be confirmed [8, 14, 15, 19]. It is relevant to question the possibility of pure nanosecond laser ablation in water. Indeed, since the nanosecond plasma, appearing picoseconds after beginning of the ns laser pulses, can readily absorb energy from the remaining portion of the laser pulse, it is, therefore, expected to be more intense (hot) then the plasma generated by a femtosecond pulse (where laser-plasma interactions may be neglected). This should, however, be confirmed with systematic measurements.

5 Conclusions

In summary, we revealed the existence of two populations of colloids, characterized by low and high size dispersions, produced by the femtosecond laser ablation from a gold target in pure water. By varying the conditions of plasma production through the target shift with respect to the focal plane of the focusing objective, we have shown that the less dispersed population is related to the radiation-related ablation of material, whereas the appearance of the more dispersed population can only be explained by the contribution of effects connected with plasma production. We propose that the target thermal heating by the plasma, or its mechanical erosion by the collapse of a plasma-induced cavitation bubble, are possible mechanisms of plasma-related ablation. A final identification of plasma-related mechanisms requires a time-resolved study of the plasma evolution. These studies are now in progress and will be published later.

ACKNOWLEDGEMENTS We thank the Natural Sciences and Engineering Research Council of Canada for funding.

REFERENCES

1 D.A. Schultz: Curr. Opin. Biotechnol. **14**, 13 (2003)
2 I. Lisiecki, M.P. Pileni: J. Am. Chem. Soc. **115**, 3887 (1993)
3 A. Fojtik, A. Henglein: Ber. Bunsen-Ges. Phys. Chem. **97**, 252 (1993)
4 J. Nedderson, G. Chumanov, T.M. Cotton: Appl. Spectrosc. **47**, 1959 (1993)
5 M. Prochazka, J. Stepanek, B. Vlckova, I. Srnova, P. Maly: J. Mol. Struct. **410**, 213 (1997)
6 F. Mafuné, J.-Y. Kohno, Y. Takeda, T. Kondow, H. Sawabe: J. Phys. Chem. B **104**, 8333 (2000)
7 F. Mafuné, J.-Y. Kohno, Y. Takeda, T. Kondow, H. Sawabe: J. Phys. Chem. B **104**, 9111 (2000)
8 F. Mafuné, J.-Y. Kohno, Y. Takeda, T. Kondow: J. Phys. Chem. B **105**, 5114 (2001)
9 F. Mafuné, J.-Y. Kohno, Y. Takeda, T. Kondow: J. Phys. Chem. B **107**, 4218 (2003)
10 Y.-H. Chen, C.S. Yeh: Coll. Surf. A **197**, 133 (2002)
11 A.V. Kabashin, M. Meunier, C. Kingston, J.H.T. Luong: J. Phys. Chem. B **107**, 4527 (2003)
12 J.-P. Sylvestre, A.V. Kabashin, E. Sacher, M. Meunier, J.H.T. Luong: J. Am. Chem. Soc. **126**, 7176 (2004)
13 J.-S Jeon, C.-S. Yeh: J. Chin. Chem. Soc. **45**, 721 (1998)
14 A.V. Simakin, V.V. Voronov, G.A. Shafeev, R. Brayner, F. Bozon-Verduraz: Chem. Phys. Lett. **348**, 182 (2001)
15 S.I. Dolgaev, A.V. Simakin, V.V. Voronov, G.A. Shafeev, F. Bozon-Verduraz: Appl. Surf. Sci. **186**, 546 (2002)

16 T. Tsuji, K. Iryo, N. Watanabe, M. Tsuji: Appl. Surf. Sci. **202**, 80 (2002)
17 T. Tsuji, T. Kakita, M. Tsuji: Appl. Surf. Sci. **206**, 314 (2003)
18 A.V. Kabashin, M. Meunier: J. Appl. Phys. **94**, 7941 (2003)
19 G. Compagnini, A.A. Scalisi, O. Puglisi: Phys. Chem. Chem. Phys. **4**, 2787 (2002)
20 J. Szejtli: Chem. Rev. **98**, 1743 (1998)
21 A. Brodeur, S.L. Chin: Phys. Rev. Lett. **80**, 4406 (1998)
22 A. Vogel, J. Noack, K. Nahen, D. Theisen, S. Busch, U. Parlitz, D.X. Hammer, G.D. Noojin, B.A. Rockwell, R. Birngruber: Appl. Phys. B **68**, 271 (1999)
23 P.K. Kennedy, D.X. Hammer, B.A. Rockwell: Prog. Quantum Electr. **21**, 155 (1997)
24 J.F. Ready, D.F. Farson, Eds.: *LIA Handbook of Laser Materials Processing* (Springer, Heidelberg 2001)
25 L.A. Chiu, A.A. Seraphin, K.D. Kolenbrander: J. Electron. Mater. **23**, 347 (1994)
26 D.B. Geohegan, A.A. Puretzky, G. Duscher, S.J. Pennycook: Appl. Phys Lett. **72**, 2987 (1998)
27 W. Liu, O. Kosareva, I.S. Golubstov, A. Iwasaki, A. Becker, V.P. Kandidov, S.L. Chin: Appl. Phys. B **76**, 215 (2003)